Available online at www.sciencedirect.com
ScienceDirect
Journal of Catalysis 250 (2007) 299–312
JOURNAL OF CATALYSIS
www.elsevier.com/locate/jcat

Self-regenerative activity of Ni/Mg(Al)O catalysts with trace Ru during daily start-up and shut-down operation of CH_4 steam reforming

Dalin Li [a], Ikuo Atake [a], Tetsuya Shishido [b], Yasunori Oumi [a], Tsuneji Sano [a], Katsuomi Takehira [a,*]

[a] *Department of Chemistry and Chemical Engineering, Graduate School of Engineering, Hiroshima University, Kagamiyama 1-4-1, Higashi-Hiroshima 739-8527, Japan*

[b] *Department of Molecular Engineering, Graduate School of Engineering, Kyoto University, Katsura 1, Nishikyo-ku, Kyoto 615-8510, Japan*

Received 22 March 2007; revised 29 May 2007; accepted 1 June 2007

Available online 2 August 2007

Abstract

Ni/Mg(Al)O catalysts doped with trace Ru showed self-regenerative activity during a daily start-up and shut-down (DSS) operation of steam reforming of methane. Formation of Ru–Ni alloy on the surface of fine Ni metal particles on the catalysts was strongly suggested by EXAFS and TPR measurements. The Ni/Mg(Al)O catalyst was passivated by the oxidative incorporation of Ni^0 to Ni^{2+} in Mg(Ni,Al)O periclase, and trace Ru assisted the regeneration of Ni metal from the Ni^{2+} by hydrogen spillover. Even notably sintered Ni metal particles on the Ni/Mg(Al)O catalyst by steaming were rapidly redispersed, resulting in the revelation of the high and stable activity during the DSS operation. The self-regeneration of the Ru–Ni/Mg(Al)O catalysts can be achieved by the continuous rebirth of active Ni metal species assisted cooperatively by both $Ni^{2+} \rightarrow Ni^0$ reduction by hydrogen-spillover via trace Ru metal or Ru–Ni alloy and reversible reduction–oxidation between Ni^0 and Ni^{2+} in Mg(Ni,Al)O periclase.

Keywords: CH_4 reforming; Daily start-up and shut-down operation; Self-regeneration; Ni/Mg(Al)O catalyst; Ru doping; Memory effect

1. Introduction

Hydrogen production for polymer electrolyte fuel cells (PEFCs) is a research area of urgent importance in addressing global warming. Steam reforming of hydrocarbons, especially of methane, is the most widespread and generally the most economical way to make hydrogen [1]. This process still requires further advances in the preparation of superior reforming catalysts, however. We previously reported that Ni/Mg(Al)O catalyst derived from hydrotalcite (HT)-like compounds produced highly dispersed and stable Ni metal particles on the surface [2–8] and have been successfully applied in the steam reforming and oxidative reforming of CH_4 [4,5].

In contrast to the large-scale use of reformers in industry under stationary operating conditions, temperature is varied frequently by daily start-up and shut-down (DSS) operations in hydrogen production for PEFCs in domestic use. Between shut-down and start-up in the DSS operation, the catalyst bed in the reformer is purged by steam to enhance safety. Thus, the catalyst must be able to tolerate multiple cycles under such unusual transient conditions without deterioration. Deactivation of Ni-loaded catalysts caused by coking, sintering, or oxidation of the active metal species have been frequently reported [9–12]. Ni metal can be oxidized not only by gaseous oxygen, but also even in the presence of steam, as reported for lanthanide-promoted sol–gel Ni/Al_2O_3 catalyst in propane steam reforming [12]. The Ni/Mg(Al)O catalysts were quickly deactivated due to the oxidation of Ni metal by both oxygen gas and steam when applied in the DSS operation of steam reforming of CH_4 [13]. The combination of trace noble metals and the Ni/Mg(Al)O catalysts has been found to be effective for suppressing Ni oxidation during the DSS operation [14,15]. For stationary operation, a similar approach has been taken for the preparation of Rh–Ni/Mg(Al)O catalyst in the partial oxidation or oxidative steam reforming of CH_4 [16,17] and noble metal–Ni/Mg(Al)O catalysts in the dry reforming of CH_4 [7]. The behavior of the Ni/MgO catalyst was improved by the addition

* Corresponding author. Fax: +81 82 424 6488.
E-mail address: takehira@hiroshima-u.ac.jp (K. Takehira).

0021-9517/$ – see front matter
doi:10.1016/j.jcat.2007.06.002

of noble metals; Rh, Pt, and Pd were successfully incorporated in the Ni/MgO catalyst for the stationary oxidative steam reforming of CH_4 [18–20]. The addition of Pt, Ir, and Ru on the Ni/γ-Al_2O_3 or Ni/$MgAl_2O_4$ catalyst resulted in an increase in metal surface area, and, moreover, the catalysts thus obtained were self-activated in the reforming reaction without prereduction [21–23].

We recently reported that the Ni/Mg(Al)O catalysts modified by trace amounts of Ru showed high and stable activity for dry reforming of methane [7]. Moreover, the Ni/Mg(Al)O catalysts with trace noble metals showed high and sustainable activity in the DSS operation of steam reforming of methane (SRM) [15] and partial oxidation of propane to synthesis gas [24,25]. In this contribution, we report excellent catalytic behavior, that is, self-regenerative activity of the Ni/Mg(Al)O catalyst with trace Ru during the DSS SRM operation. The self-regeneration was observed not only for the fresh catalyst, but also for the severely sintered catalyst after the steaming treatment. Effects of the doping of trace Ru as well as the reversible reduction–oxidation between $Ni^0 \leftrightarrow Ni^{2+}$ in Mg(Ni,Al)O periclase on the self-regeneration of active Ni species on the Ni/Mg(Al)O catalysts were carefully investigated.

2. Experimental

2.1. Catalyst preparation

Ni-loaded Mg(Al)O catalyst with the Mg/Ni/Al composition of 2.5/0.5/1 was prepared by co-precipitation as described previously [2–8]. $Mg_{2.5}(Ni_{0.5})$–Al HT-like precursor, in which a part of Mg^{2+} in Mg–Al HT was replaced by Ni^{2+}, was prepared by co-precipitation of the nitrates of the metal components. An aqueous solution containing the nitrates of Mg^{2+}, Ni^{2+}, and Al^{3+} was added slowly into an aqueous solution of sodium carbonate at room temperature. Simultaneously, the pH of the solution was adjusted to 10.0 by adding an aqueous solution of sodium hydroxide under vigorous stirring. During the mixing treatment, a heavy slurry precipitated. The crystal growth occurred by aging the solution at 60 °C for 12 h. After the solution was cooled to room temperature, the precipitate was washed with deionized water and dried in air at 100 °C. The $Mg_{2.5}(Ni_{0.5})$–Al HT-like precursor was calcined in a muffle furnace in a static air atmosphere by increasing the temperature from ambient temperature to 850 °C at a rate of 0.83 °C min^{-1} and maintaining it at 850 °C for 5 h, to form $Mg_{2.5}(Al,Ni_{0.5})O$ periclase as the precursor of the $Ni_{0.5}/Mg_{2.5}(Al)O$ catalyst. The periclase materials were obtained as powders, and Ni loading was 16.0 wt% by inductively coupled plasma spectroscopy (ICP) analyses after calcination at 850 °C.

Ru loading was done by adopting a "memory effect" of Mg(Ni)–Al HT [14]; a 1.0 g portion of $Mg_{2.5}(Al,Ni_{0.5})O$ periclase powder was dipped in an aqueous solution of Ru(III) nitrate for 1 h at room temperature, followed by drying in air at 100 °C. A prescribed amount of Ru(III) nitrate was dissolved in 5 ml of deionized water unless specifically mentioned otherwise. The dipping and drying treatment caused Mg(Ni)–Al HT to be reconstituted from $Mg_{2.5}(Ni_{0.5},Al)O$ periclase due to the "memory effect." During this reconstitution, Ru was physically trapped in the layered structure of the HT. The sample was finally calcined at 850 °C for 5 h to form the precursor of the Ru–$Ni_{0.5}/Mg_{2.5}(Al)O$ catalysts. The precursor powder was pressed into a disc, crushed roughly, and sieved to particle sizes of 0.36–0.60 mm in diameter for use in the reforming reactions.

Also as a control, 13.5 wt% Ni/γ-Al_2O_3 catalyst was prepared by the incipient wetness method using γ-Al_2O_3 (ALO8) and an aqueous solution of Ni(II) nitrate, followed by calcination at 850 °C for 5 h. Commercial Ni and Ru catalysts, supplied from Süd-Chemie Catalysts Japan, were used as controls. FCR (12 wt% Ni/α-Al_2O_3) and RUA (2 wt% Ru/α-Al_2O_3) catalysts as received were first crushed to fine powder, pressed into discs, crushed roughly, and sieved to particle sizes of 0.36–0.60 mm in diameter for use in the reforming reactions.

2.2. Catalyst characterization

The structure of the catalysts was studied by using powder X-ray diffraction (XRD), scanning electron microscopy (SEM), transmission electron microscopy (TEM), X-ray absorption (XANES and EXAFS), ICP, temperature-programmed reduction (TPR), temperature-programmed oxidation (TPO), and N_2 and H_2 adsorption. XRD was recorded on a Mac Science MX18XHF-SRA powder diffractometer with monochromatized Cu$K\alpha$ radiation ($\lambda = 0.154$ nm) at 40 kV and 30 mA. The diffraction pattern was identified through comparison with those included in the JCPDS (Joint Committee of Powder Diffraction Standards) database. A particle size of Ni metal on the catalyst was calculated from Scherrer's equation: $d = K\lambda/\beta\cos\theta$; β, full width at half maximum; $K = 0.94$ and $\lambda = 1.5405$ Å.

SEM measurements were performed with a JEOL JEM-6320F microscope using a Noran Voyager energy dispersive X-ray spectroscope at an accelerating voltage of 300 kV. TEM images were obtained on a JEOL JEM-2010 microscope operated at 200 kV. The samples were crushed to fine powders, dispersed in ethanol using supersonic waves, and deposited on a Cu TEM grid with a holey carbon film.

Ni K-edge and Ru K-edge EXAFS were measured at the BL01B1 station of the SPring-8 with the approval of the Japan Synchrotron Radiation Research Institute (JASRI) (proposal 2006A1217). The storage ring was operated at 8 GeV with a ring current of 98–100 mA. A double-mirror system was used to avoid higher harmonics in the X-ray beam. A Si(111) single crystal was used to obtain a monochromatic X-ray beam. Ni K-edge EXAFS spectra were measured in transmission mode using two ion chambers filled with N_2 (I_0) and 25% Ar diluted with N_2 (I). Ru K-edge EXAFS spectra were measured in transmission and fluorescence modes using ion chambers [50% Ar diluted with N_2 (I_0) and 75% Ar diluted with Kr (I)] and a Lytle detector (100% Kr), respectively. Analyses of EXAFS data were performed using the REX2000 program (version: 2.3.3; Rigaku Corp.). For EXAFS analyses, the oscillation was first extracted from EXAFS data using a spline-smoothing method [26]. The oscillation was normalized by a edge height ca. 50 eV higher than the adsorption edge. For the curve-fitting

analysis, the empirical phase shift and amplitude functions for the Ni–Ni and Ru–Ru bonds were extracted from data for Ni and Ru foils. Theoretical functions for the Ru–Ni, Ni–O, and Ru–O bonds were calculated using the FEFF8.2 program [27]. The 0.50 wt% Ru-doped $Ni_{0.5}/Mg_{2.5}(Al)O$ sample was used for this measurement to guarantee accuracy of the analytical results.

ICP measurement was performed with a Seiko SPS 7700. The content of each metal component was determined after the sample was completely dissolved using diluted hydrochloric acid and a small amount of hydrofluoric acid.

TPR of the catalyst was performed at a heating rate of 10 °C min^{-1} using a H_2/Ar (5/95 ml min^{-1}) mixed gas as the reducing gas after passing through a 13X molecular sieve trap to remove water. A U-shaped quartz tube reactor (6 mm i.d.) equipped with a thermal conductivity detector for monitoring H_2 consumption was used. Before the TPR measurements, the sample was calcined at 300 °C for 2 h in an O_2/Ar (10/40 ml min^{-1}) mixed gas.

The N_2 adsorption (−196 °C) study was conducted to examine the BET surface area of the samples after the calcination. The measurement was carried out on a Bell-Japan Belsorp-mini. The samples were pretreated in N_2 at 200 °C for 10 h before the measurements were obtained.

Ni dispersion was determined by static equilibrium adsorption of H_2 at ambient temperature using the pulse method. A 50-mg catalyst sample was reduced at 900 °C in a H_2/N_2 (5/20 ml min^{-1}) mixed gas for 1 h, and this reduced catalyst was used for the measurement. During the pulse experiment, the amount of H_2 was monitored by a TCD gas chromatograph. Uptake of H_2 at monolayer coverage of the Ni species was used to estimate Ni metal dispersion and particle size. The equation used to calculate dispersion was

$$\%D = 1.17X/Wf, \tag{1}$$

where X is H_2 uptake in μmol g^{-1} of catalyst, W is the weight percent of nickel, and f is the fraction of nickel reduced to the metal, assumed to be 80% for the HT-derived catalysts [15] and 100% for the impregnated catalyst. The average crystallite diameters, d, were calculated from $\%D$, assuming spherical metal crystallites [28],

$$d = 971/(\%D). \tag{2}$$

2.3. Kinetic measurements

Steam reforming of methane was conducted in a fixed-bed flow reactor with a $CH_4/H_2O/N_2$ (50/100/25 ml min^{-1}) mixed gas at 700 °C over a 50-mg catalyst sample in a DSS-like mode (Fig. 1). The catalyst was used as particles (0.36–0.60 mm in diameter) dispersed in 50 mg of quartz beads. A U-shaped quartz reactor was used, with the catalyst bed near the bottom. N_2 was used as an internal standard for calculating the methane conversion and the product yields. After the catalyst was prereduced in a H_2/N_2 (5/25 ml min^{-1}) mixed gas at 900 °C for 30 min, the reaction was started at 700 °C. After 90 min of reaction at 700 °C, the reactor was cooled to 200 °C under steam purging

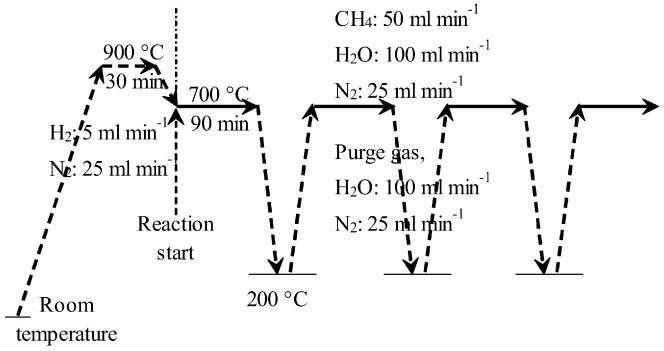

Fig. 1. DSS-like operation mode in steam reforming of methane.

with a H_2O/N_2 (100/25 ml min^{-1}) mixed gas. The reactor was maintained at 200 °C for 30 min, after which the temperature was again increased to 700 °C still under the purging conditions. When the temperature reached 700 °C, the reaction was again started by adding methane (50 ml min^{-1}) into the purging gas. The reaction was carried out at 700 °C for 90 min, followed by steam purging. Thus the cycle reaction was repeated four times to perform the DSS-like operation. The thermocouple to control the reaction temperature was placed at the center of the catalyst bed. In each SRM step at 700 °C, analyses of product gases were started by online TCD-gas chromatography 30 min after starting the SRM when the gas flow of the $CH_4/H_2O/N_2$ mixture was stabilized.

Steaming treatment of the catalyst was carried out using the fixed-bed flow reactor in a $H_2/H_2O/N_2$ (20/100/25 ml min^{-1}) mixed gas flow for 10 h at 900 or 850 °C. Each 300 mg of the catalyst was steamed, and a 50-mg catalyst sample after steaming was used for the catalytic reaction in both the stationary and DSS operations of SRM. The stationary operation was conducted in a $CH_4/H_2O/N_2$ (50/100/25 ml min^{-1}) mixed gas flow at 700 °C for 180 min, and the DSS operation was conducted as described above.

Turnover frequency was evaluated using the catalysts as powders, because the activity of the $Ni_{0.5}/Mg_{2.5}(Al)O$-based catalyst was so high that only a small amount of catalyst was needed to precisely measure the reaction rate in our small reactor. The reaction had to be carried out without channeling in the catalyst bed at low methane conversion and very high space velocity. All catalysts were crushed, and a 10 mg portion of the catalyst powders (0.075–0.180 mm in diameter) was dispersed in ca. 20 mg of quartz wool and pretreated in a H_2/N_2 (5/25 ml min^{-1}) mixed gas flow at 900 °C for 30 min. The reaction was carried out at either 500 or 600 °C in a $CH_4/H_2O/N_2$ (88.8/177.6/44.4 ml min^{-1}) mixed gas flow at a GHSV of 1.6×10^6 ml g$_{cat}^{-1}$ h^{-1}. For both the FCR and RUA catalysts, the reaction was carried out at a low GHSV of 3.6×10^5 ml g$_{cat}^{-1}$ h^{-1}, due to their low activity.

3. Results

3.1. Morphology of Ru-doped Ni/Mg(Al)O catalysts

SEM images of the 0.10 wt% Ru–$Ni_{0.5}/Mg_{2.5}(Al)O$ catalyst during preparation are shown in Fig. 2. After the powders of

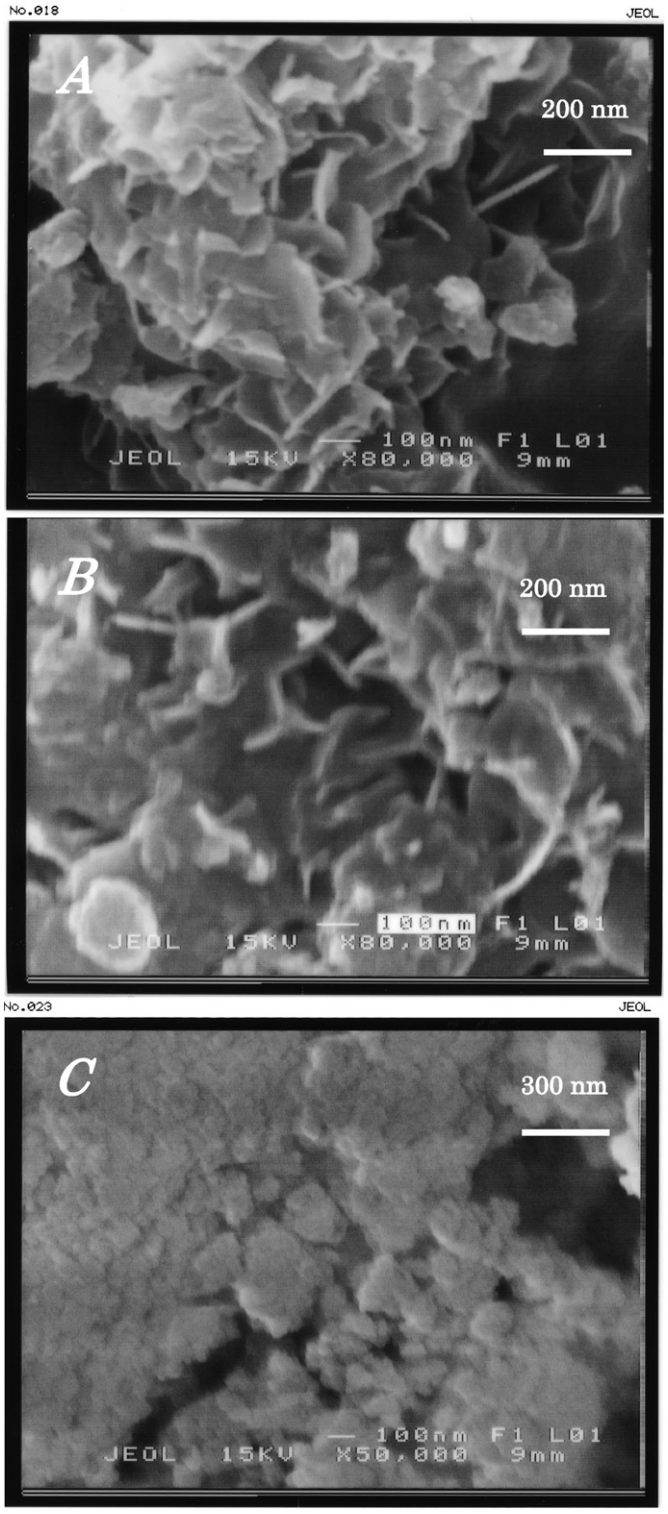

Fig. 2. SEM images of the 0.10 wt% Ru-$Ni_{0.5}/Mg_{2.5}$(Al)O catalyst during the preparation. (A) After dipping, followed by drying; (B) after calcination at 850 °C; (C) after reduction at 900 °C.

$Mg_{2.5}(Ni_{0.5},Al)O$ periclase were dipped in an aqueous solution of Ru(III) nitrate, followed by drying, the precursors showed worm-like surface morphology (Fig. 2A), which remained after calcination at 850 °C (Fig. 2B). We previously reported that such worm-like surface morphology appeared during the preparation of eggshell-type loaded Ni/Mg(Al)O catalysts [8]. We confirmed that the HT-like layered structure was reconstituted during the dipping and affected the surface morphology of Mg(Ni,Al)O periclase even after calcination, although no HT-like structure remained. After the reduction at 900 °C, such worm-like morphology totally disappeared, and agglomerates of particles were observed (Fig. 2C). After the reduction, Ni^{2+} in Mg(Ni,Al)O periclase was reduced to Ni metal and migrated to the surface of the particles, resulting in the destruction of the framework derived from the HT-like layered structure. Finally, the worm-like morphology derived from the HT structure was completely demolished.

3.2. Activity of Ru-doped Ni/Mg(Al)O catalysts in the DSS operation

We previously reported that Ru doping enhanced the sustainability of the $Ni_{0.5}/Mg_{2.5}$(Al)O catalyst during SRM in the DSS-like operation [15]. The results of the SRM DSS operation over the 0.1 wt% Ru–$Ni_{0.5}/Mg_{2.5}$(Al)O catalyst, as well as the other catalysts, are shown in Fig. 3. The SRM always proceeded selectively to H_2, CO, and CO_2 following the thermodynamic equilibrium under the condition of S/C = 2/1. We compared the activity by methane conversion. The $Ni_{0.5}/Mg_{2.5}$(Al)O catalyst was completely deactivated; that is, methane conversion decreased from that of thermodynamic equilibrium to zero just after the first steam purging. Such deactivation was due to the oxidation of Ni metal on the catalyst surface [13]. A sudden decrease in methane conversion after the first steam purging also was observed for the other supported Ni catalysts (13.5 wt% Ni/γ-Al_2O_3 and FCR). The activity of the RUA catalyst was a little lower than that of the 0.1 wt% Ru–$Ni_{0.5}/Mg_{2.5}$(Al)O catalyst but was stable during the DSS operation. After deactivation, reflection lines of NiO appeared for both the 13.5 wt% Ni/γ-Al_2O_3 and FCR catalysts, whereas no reflection of NiO was detected but reflections of Mg(Ni,Al)O periclase were enhanced for the $Ni_{0.5}/Mg_{2.5}$(Al)O catalyst [13]. This indicates that Ni metal was oxidized to Ni^{2+} and incorporated into the Mg(Ni,Al)O periclase. In contrast, RUA deactivation was likely due not to such a sudden oxidation of Ru metal, but rather to carbon deposition on the catalyst or sintering of Ru metal. Among the catalysts tested, the 0.10 wt% Ru–$Ni_{0.5}/Mg_{2.5}$(Al)O catalyst alone showed stable activity during the SRM DSS, indicating that trace Ru doping suppressed the oxidation of Ni metal or quickly rereduced Ni^{2+} into Ni metal under SRM atmosphere.

Effects of a doping amount of Ru on the activity of the Ru–$Ni_{0.5}/Mg_{2.5}$(Al)O catalysts are shown in Fig. 4. The doping of 0.01 wt% was not effective due to too small amount; the activity was quickly lost even after the first steam purging and Ni oxidation simultaneously took place on the catalyst surface. The doping above 0.05 wt% stabilized the catalytic activity. With increasing Ru doping, the activity was more efficiently stabilized; more intensive Ni metal reflections were observed in the XRD patterns of the catalysts after the SRM DSS. As observed in Fig. 4, methane conversion decreased slightly just after the steam purging, and, moreover, the decrease was enhanced with decreasing Ru doping and was magnified by repeating the steam

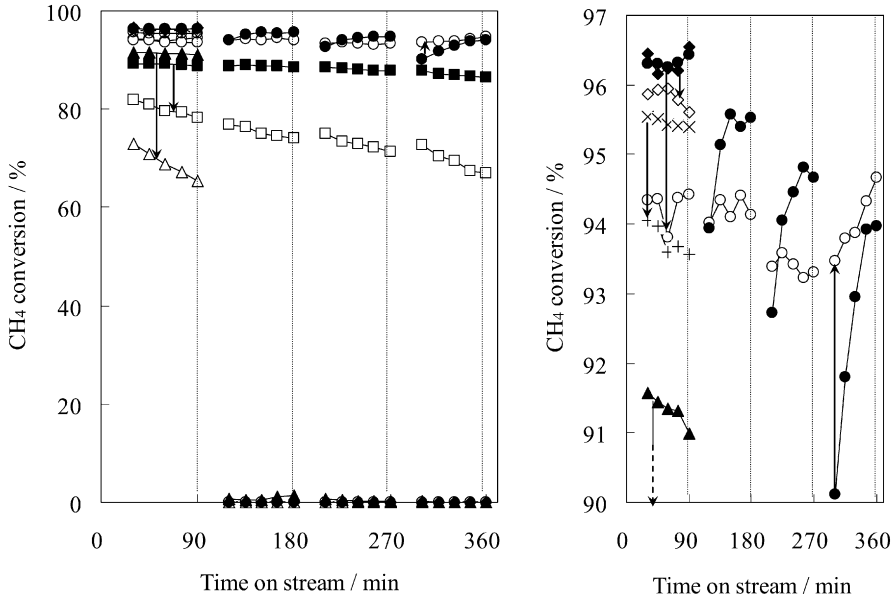

Fig. 3. Comparison of the activity of supported Ni and Ru catalysts before and after steaming at 900 °C for 10 h in the steam purged SRM DSS. Reaction conditions: $CH_4/H_2O/N_2 = 50/100/25$ ml min^{-1}; 700 °C; catalyst, 50 mg. 0.10 wt% Ru–$Ni_{0.5}/Mg_{2.5}$(Al)O, before (●), after (○); $Ni_{0.5}/Mg_{2.5}$(Al)O, before (×), after (+); 13.5 wt% Ni/γ-Al_2O_3, before (♦), after (◊); RUA, before (■), after (□); FCR, before (▲), after (△).

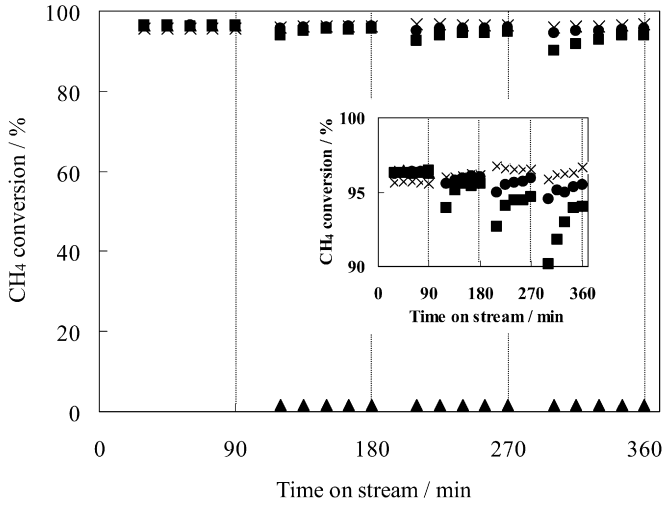

Fig. 4. Methane steam reforming over Ru–$Ni_{0.5}/Mg_{2.5}$(Al)O catalysts under the steam purged SRM DSS conditions. Reaction conditions: $CH_4/H_2O/N_2 = 50/100/25$ ml min^{-1}; 700 °C; catalyst, 50 mg. (▲) 0.01 wt% Ru–$Ni_{0.5}/Mg_{2.5}$(Al)O; (■) 0.05 wt% Ru–$Ni_{0.5}/Mg_{2.5}$(Al)O; (●) 0.10 wt% Ru–$Ni_{0.5}/Mg_{2.5}$(Al)O; (×) 0.50 wt% Ru–$Ni_{0.5}/Mg_{2.5}$(Al)O.

purging. The decreased methane conversion was due to the oxidation of surface Ni metal into Ni^{2+} in Mg(Ni,Al)O periclase. It is likely that reduction–oxidation between Ni^0 and Ni^{2+} reversibly worked on the surface of active Ru–Ni/Mg(Al)O catalyst during the steam-purged SRM DSS.

3.3. Effect of steaming on Ru-doped Ni/Mg(Al)O catalysts

The physicochemical properties of supported Ni and Ru catalysts before and after the steaming in a $H_2/H_2O/N_2$ (20/100/25 ml min^{-1}) mixed gas flow for 10 h at 900 °C are given in Table 1. It is known that such steaming treatment causes a severe sintering of supported metal catalysts and is often used to conventionally evaluate the catalyst life. It is said that the aforementioned steaming conditions correspond to catalyst testing for ca. 5000 h in the actual reformer. After the steaming, specific surface areas of the $Ni_{0.5}/Mg_{2.5}$(Al)O, 13.5 wt% Ni/γ-Al_2O_3, and 0.10 wt% Ru–$Ni_{0.5}/Mg_{2.5}$(Al)O catalysts decreased significantly, whereas those of both FCR and RUA catalysts showed no substantial decrease; both commercial catalysts are stabilized considering their uses in the actual reformer. H_2 uptake also decreased significantly, indicating a decrease in the Ni dispersion or an increase in the Ni metal particle size. The increase in the Ni metal particle size was also confirmed by the calculation from the line width in the XRD reflections. Both FCR and RUA catalysts showed extremely small and undetectable values in the H_2 uptake before and after steaming, respectively. Particle sizes of Ni and Ru metals calculated from the XRD data on both FCR and RUA catalysts showed no remarkable increase by the steaming treatment. For both $Ni_{0.5}/Mg_{2.5}$(Al)O and 0.10 wt% Ru–$Ni_{0.5}/Mg_{2.5}$(Al)O catalysts, the steaming was carried out also at 850 °C for 10 h (Table 1); the decreases in both surface area and H_2 uptake were a little moderated compared with that at 900 °C, but still remarkable sintering took place on both catalysts.

It was often reported that Ni loading on γ-Al_2O_3 afforded highly dispersed Ni metal particles via a formation of $NiAl_2O_4$ spinel on the catalyst surface [29]. However, on the 13.5 wt% Ni/γ-Al_2O_3 catalyst, Ni dispersion was lower, whereas Ni metal particle size was larger compared with the $Ni_{0.5}/Mg_{2.5}$(Al)O and 0.10 wt% Ru–$Ni_{0.5}/Mg_{2.5}$(Al)O catalysts before the steaming. In the results obtained by both XRD mea-

Table 1
Physicochemical properties of supported metal catalysts before and after the steaming[a]

Catalyst	BET surface area[b] ($m^2\ g_{cat}^{-1}$)		H_2 uptake[c] ($\mu mol\ g_{cat}^{-1}$)		Dispersion[d] (%)		Particle size of Ni (Ru) metal (nm)				
							XRD[e]			H_2 uptake[f]	
	Before	After	Before	After	Before	After	Before	After	After[g]	Before	After
$Ni_{0.5}/Mg_{2.5}(Al)O$	173.6	56.8	120.7	40.2	13.1	4.4	6.8	18.4	n.d.	7.4	22.3
	–	75.6[h]	–	39.9[h]	–	4.3[h]	–	14.4[h]	–	–	22.5[h]
13.5 wt% $Ni/\gamma\text{-}Al_2O_3$	106.8	61.0	74.4	19.3	8.1[i]	2.1[i]	9.0	21.0	n.d.	12.0[i]	46.4[i]
0.1 wt% $Ru–Ni_{0.5}/Mg_{2.5}(Al)O$	128.7	56.4	221.9	58.4	24.0	6.3	5.2	16.8	8.3	4.0	15.3
	–	70.5[h]	–	95.3[h]	–	10.3[h]	–	14.1[h]	–	–	9.4[h]
FCR	12.3	11.7	0.08	–	0.0	–	23.1	24.3	26.1	–	–
RUA	11.4	10.6	0.18	-	0.1	–	(23.6)	(25.6)	(37.0)	–	–

[a] Steaming was carried out at 900 or 850 °C[h] for 10 h in a mixed gas flow of $H_2/H_2O/N_2$ (20/100/25 ml min^{-1}).
[b] The catalysts were calcined at 850 °C for 5 h before catalytic tests.
[c] Determined by the H_2 pulse method.
[d] Calculated from the H_2 uptake assuming the reduction degree of 80% for hydrotalcite derived catalyst [15,31] and 100% for impregnated catalyst.[i]
[e] Calculated from the full width at half maximum of the reflections of Ni (200) and Ru (101) planes in the XRD using the Scherrer equation.
[f] Calculated using the equation: $d = 971/(\%D)/10$ where D is the dispersion [28].
[g] After steaming at 900 °C, followed by the steam purged SRM DSS operation between 200 and 700 °C.

surement and H_2 uptake after the steaming, Ni metal sintering was the most significant on the 13.5 wt% $Ni/\gamma\text{-}Al_2O_3$, followed by the $Ni_{0.5}/Mg_{2.5}(Al)O$ and then by the 0.10 wt% Ru–$Ni_{0.5}/Mg_{2.5}(Al)O$ catalysts. Although significant increase was observed by the 0.10 wt% Ru doping on the $Ni_{0.5}/Mg_{2.5}(Al)O$ catalyst, the contribution of Ru in H_2 uptake must be negligible, since a chemisorption stoichiometry is $H/Ru_s = 1/1$ [30] and the molar ratio of Ru/Ni on the 0.10 wt% Ru–$Ni_{0.5}/Mg_{2.5}(Al)O$ catalyst is calculated as 1/275 of total Ni amount, or at least 1/220 for surface Ni amount calculated from 80% of Ni reduction degree [15,31]. Even supposing that all Ru species located on the surface of Ni metal particles, direct contribution of Ru on the H_2 uptake must be small; the other factor such as surface RuNi alloy formation or decrease in the size of Ni metal particles must be considered for explaining the increase in the H_2 uptake by the Ru doping. It is concluded that the Ru doping on the $Ni_{0.5}/Mg_{2.5}(Al)$ catalyst certainly suppressed the sintering of Ni metal particles during the steaming treatment.

3.4. Activity of Ru-doped Ni/Mg(Al)O catalysts after the steaming

Stationary SRM operation was carried out at 700 °C over the supported Ni and Ru catalysts before and after steaming at 900 °C; the effects of the steaming on the catalyst deactivation were compared (Fig. 5). The most severe deactivation took place on the FCR, followed by the RUA and then by the $Ni_{0.5}/Mg_{2.5}(Al)O$ catalysts. Both FCR and RUA catalysts showed a gradual decrease in methane conversion during the reaction. The $Ni_{0.5}/Mg_{2.5}(Al)O$ catalyst was less sustainable than the 13.5 wt% $Ni/\gamma\text{-}Al_2O_3$ catalyst against the steaming, probably due to the presence of MgO in the former catalyst, since MgO is thermodynamically unstable compared with $Mg(OH)_2$ under steam atmosphere [32]. MgO reacts easily even with moisture in the air, especially at low coordination atomic sites, to form $Mg(OH)_2$ brucite, leading to surface modification and further to deactivation of the $Ni_{0.5}/Mg_{2.5}(Al)O$ catalyst. The most stable activity was obtained over the 0.10 wt% Ru–$Ni_{0.5}/Mg_{2.5}(Al)O$ catalyst; the deactivation was negligibly small although extremely gradual decrease took place in methane conversion (Fig. 5).

Further, SRM DSS was carried out between 200 and 700 °C under steam purging conditions over the catalysts after steaming at 900 °C (Fig. 3). The deactivation by steaming was most enhanced for the FCR, followed by the $Ni_{0.5}/Mg_{2.5}(Al)O$ and the 13.5 wt% $Ni/\gamma\text{-}Al_2O_3$ catalyst and all these supported Ni catalysts again showed a total deactivation just after the 1st steam purging. The RUA catalyst was deactivated by steaming but showed no total deactivation; the activity gradually decreased during the DSS operation irrespective of each steam purging. Among the catalysts tested, the 0.10 wt% Ru–$Ni_{0.5}/Mg_{2.5}(Al)O$ catalyst alone showed a stable activity during the SRM DSS. Judging from the time course of methane conversion during the DSS operation (Fig. 3, magnified), interestingly it seems that the activity of the 0.10 wt% Ru–$Ni_{0.5}/Mg_{2.5}(Al)O$ catalyst was rather stabilized after the steaming; a slight decrease in the methane conversion observed just after the steam purging disappeared and the methane conversion became almost constant throughout the DSS operation after the steaming.

The results obtained above indicate that all supported Ni catalysts tested were absolutely inadequate for the DSS operation except the 0.10 wt% Ru–$Ni_{0.5}/Mg_{2.5}(Al)O$ catalyst. Although the 13.5 wt% $Ni/\gamma\text{-}Al_2O_3$ catalyst showed a stable activity in the steady state operation even after the steaming (Fig. 5), it was not tolerant in the DSS operation. The deactivation of these Ni catalysts is not due to the sintering but surely due to the oxidation of Ni metal to NiO as seen in the XRD patterns after steaming at 900 °C followed by the SRM DSS (vide infra). Exceptionally, the RUA catalyst showed a stable activity in the DSS operation, but was deactivated significantly after steaming. This deactivation is probably due to the sintering (vide infra) or the surface passivation of Ru metal particles by steam, since no significant coking took place on the catalyst. We frequently observed this type of deactivation of supported Ru catalysts under steam or air atmosphere, suggesting the Ru is not stable as the

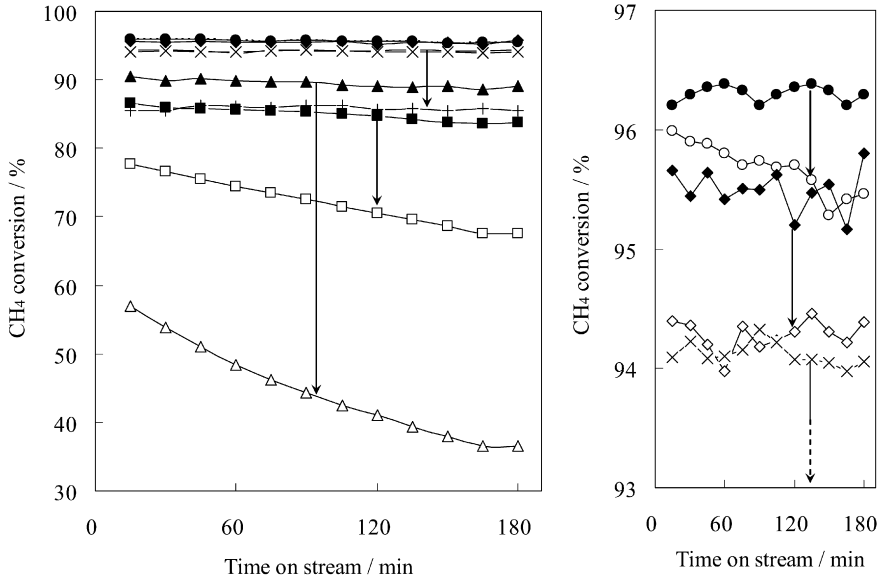

Fig. 5. Comparison of the activity of supported Ni and Ru catalysts before and after steaming at 900 °C for 10 h in the SRM under steady state conditions. Reaction conditions: $CH_4/H_2O/N_2 = 50/100/25$ ml min^{-1}; 700 °C; catalyst, 50 mg. 0.10 wt% Ru–$Ni_{0.5}/Mg_{2.5}$(Al)O, before (●), after (○); $Ni_{0.5}/Mg_{2.5}$(Al)O, before (×), after (+); 13.5 wt% Ni/γ-Al_2O_3, before (♦), after (◊); RUA, before (■), after (□); FCR, before (▲), after (△).

other noble metals, such as Pt and Rh. It must be emphasized that, even after steaming, the 0.1 wt% Ru–$Ni_{0.5}/Mg_{2.5}$(Al)O catalyst alone showed a high and stable activity not only in the stationary operation but also in the DSS operation.

3.5. Coking on Ru-doped Ni/Mg(Al)O catalysts

Deactivation of supported Ni catalysts took place either by coking on the catalysts or by sintering or oxidation of active Ni metal particles. Although remarkable sintering of Ni metal particles was observed over all $Ni_{0.5}/Mg_{2.5}$(Al)O, 0.10 wt% Ru–$Ni_{0.5}/Mg_{2.5}$(Al)O, and 13.5 wt% Ni/γ-Al_2O_3 catalysts after the steaming (Table 1), these catalysts showed no severe deactivation. Contrarily both RUA and FCR catalysts afforded significant deactivation although no distinct sintering took place over them (Fig. 5).

TPO was carried out for the supported Ni and Ru catalysts passivated by steaming followed by the SRM at 700 °C operated under stationary conditions (Fig. 5) and the results are shown in Fig. 6. Carbon dioxide alone was produced and no other compound was detected during the TPO. The amount of coke materials calculated from the total amount of carbon dioxide produced was as follows: RUA, 0.04 wt%; FCR, 0.46 wt%; 13.5 wt% Ni/γ-Al_2O_3, 0.11 wt%; $Ni_{0.5}/Mg_{2.5}$(Al)O, 0.70 wt% and 0.10 wt% Ru–$Ni_{0.5}/Mg_{2.5}$(Al)O, 0.89 wt%. The RUA catalyst showed only slight coking, whereas all of the supported Ni catalysts but 13.5 wt% Ni/γ-Al_2O_3 exhibited enhanced coking. Ru doping was not effective for suppressing coking on the $Ni_{0.5}/Mg_{2.5}$(Al)O catalyst, probably due an insufficient amount of Ni (1/275 mol), indicating that the active site was metallic Ni on the 0.10 wt% Ru–$Ni_{0.5}/Mg_{2.5}$(Al)O catalyst. The pattern of CO_2 formation during TPO depended in large part on the type of catalyst used. Both $Ni_{0.5}/Mg_{2.5}$(Al)O and 0.10 wt% Ru–$Ni_{0.5}/Mg_{2.5}$(Al)O showed similar patterns of CO_2 formation, with formation starting at low temperature and several peaks

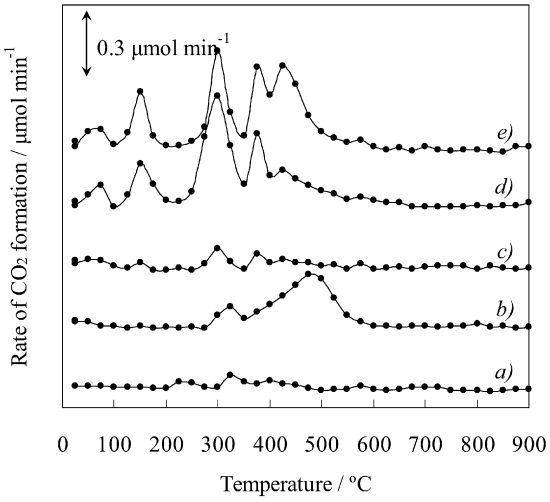

Fig. 6. TPO profiles of the supported Ni and Ru catalysts passivated by steaming at 900 °C after followed by the steady state SRM. (a) RUA; (b) FCR; (c) 13.5 wt% Ni/γ-Al_2O_3; (d) $Ni_{0.5}/Mg_{2.5}$(Al)O; (e) 0.10 wt% Ru–$Ni_{0.5}/Mg_{2.5}$(Al)O.

appearing with increasing temperature. It has been reported that graphite-like coke ignited at higher temperature around 500 °C, whereas either reactive carbonaceous deposit or chemisorbed CO present on the surface after terminating reaction ignited at temperatures below 400 °C [33]. Note that MgO as the Ni catalyst support accelerated the formation of reactive surface carbon even though it suppressed coking on the catalyst [33].

The significant CO_2 formation observed in the TPO of the FCR catalyst at around 500 °C is probably due to the formation of graphitic carbon. Although the possibility of deactivation by coking due to the formation of graphitic carbon cannot be excluded, another mechanism (e.g., surface oxidation of Ni metal particles) must be considered for the FCR catalyst. On both

the $Ni_{0.5}/Mg_{2.5}(Al)O$ and 0.1 wt% Ru–$Ni_{0.5}/Mg_{2.5}(Al)O$ catalysts, CO_2 formation was not significant at around 500 °C and observed mainly at low temperature in the TPO. The amount of coke was the highest and the deactivation the lowest on the 0.10 wt% Ru–$Ni_{0.5}/Mg_{2.5}(Al)O$ catalyst. Likely because the fact that the coke material formed on the 0.10 wt% Ru–$Ni_{0.5}/Mg_{2.5}(Al)O$ catalyst was not graphitic, and more reactive carbonaceous materials that can be gasified through the DSS operation.

3.6. TOF of Ru-doped Ni/Mg(Al)O catalysts

TOF of the supported Ni catalyst was calculated based on both surface Ni amount and total Ni amount. The results are shown in Table 2, together with those for the RUA catalyst. The activities of the catalysts before and after steaming were roughly compared based on the methane conversion (Figs. 3 and 5). However, the methane conversions observed over the $Ni_{0.5}/Mg_{2.5}(Al)O$-based catalysts were always close to the thermodynamic equilibrium and could not be compared precisely. A more precise measurement of catalytic activity must be obtained based on the TOF of the catalyst. To measure the TOF values of these catalysts, the catalyst samples had to be crushed into powders as described in the Experimental section. Therefore, the order of the activity of the catalysts obtained with the powders differed from those obtained with the particles (Figs. 3 and 5). According to the results of the TOF measurements (Table 2), the 13.5 wt% Ni/γ-Al_2O_3 catalyst was the most severely deactivated, followed by $Ni_{0.5}/Mg_{2.5}(Al)O$ and the 0.10 wt% Ru–$Ni_{0.5}/Mg_{2.5}(Al)O$. Because the amount of surface metal could not be accurately determined by H_2 pulse measurements, TOF values were calculated based on the total metal amount over both the FCR and RUA catalysts. Their TOF values were one unit smaller than those of the $Ni_{0.5}/Mg_{2.5}(Al)O$-based catalysts; moreover, heavy deactivation occurred on the commercial catalysts by steaming. Note that the TOF value of the 0.1 wt% Ru–$Ni_{0.5}/Mg_{2.5}(Al)O$ catalyst alone showed no significant decrease even after the steaming treatment.

3.7. XRD patterns of Ru-doped Ni/Mg(Al)O catalysts after steaming

XRD patterns of both the $Ni_{0.5}/Mg_{2.5}(Al)O$ and 0.10 wt% Ru–$Ni_{0.5}/Mg_{2.5}(Al)O$ catalysts before and after steaming at 900 °C are shown in Fig. 7. It can be clearly seen that reflection

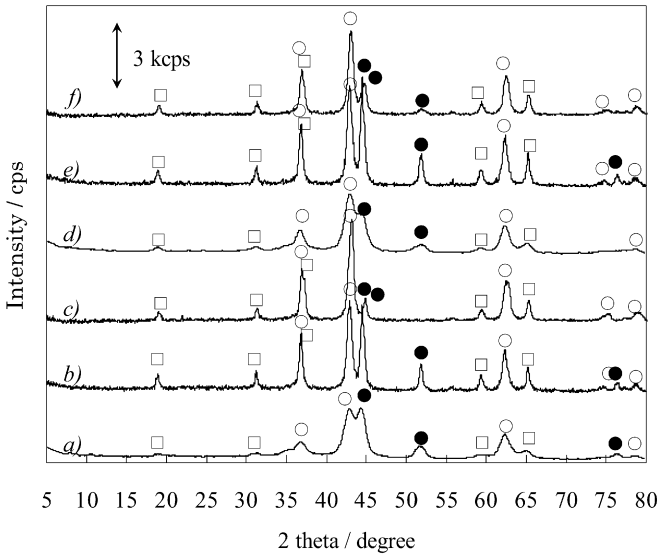

Fig. 7. XRD patterns of $Ni_{0.5}/Mg_3(Al)O$ and 0.10 wt% Ru–$Ni_{0.5}/Mg_{2.5}(Al)O$ catalysts after the reduction, after the steaming at 900 °C and after further followed by the steam purged SRM DSS. (a) $Ni_{0.5}/Mg_{2.5}(Al)O$ after reduction; (b) $Ni_{0.5}/Mg_{2.5}(Al)O$ after steaming at 900 °C; (c) (b) $Ni_{0.5}/Mg_{2.5}(Al)O$ after teaming at 900 °C followed by the SRM DSS; (d) 0.10 wt% Ru–$Ni_{0.5}/Mg_{2.5}(Al)O$ after reduction; (e) 0.10 wt% Ru–$Ni_{0.5}/Mg_{2.5}(Al)O$ after steaming at 900 °C; (f) 0.10 wt% Ru–$Ni_{0.5}/Mg_{2.5}(Al)O$ after steaming at 900 °C followed by the SRM DSS. (○) Mg(Ni,Al)O periclase; (□) $Mg(Ni)Al_2O_4$ spinel; (●) Ni metal.

Table 2
Turn over frequency of supported Ni and Ru catalysts before and after steaming [a,b]

Before or after	Catalyst	CH_4 conversion (%)		H_2 uptake ($\mu mol\ g_{cat}^{-1}$)	TOF-s[c] (s^{-1})		TOF-t[d] (s^{-1})	
		500 °C	600 °C		500 °C	600 °C	500 °C	600 °C
Before	$Ni_{0.5}/Mg_{2.5}(Al)O$[e]	14.6	43.5	163.2	2.95	8.81	0.35	1.06
	13.5 wt% Ni/γ-Al_2O_3[e]	9.35	29.3	71.1	4.35	13.6	0.27	0.84
	0.10 wt% Ru–$Ni_{0.5}/Mg_{2.5}(Al)O$[e]	12.8	37.7	213.4	1.99	5.84	0.31	0.93
	FCR[f]	3.55	29.3	–	–	–	0.03	0.08
	RUA[f]	7.13	25.3	–	–	–	0.54	1.90
After	$Ni_{0.5}/Mg_{2.5}(Al)O$[e]	5.42	25.9	26.6	6.73	32.1	0.13	0.63
	13.5 wt% Ni/γ-Al_2O_3[e]	3.75	11.9	24.0	5.16	16.3	0.09	0.29
	0.10 wt% Ru–$Ni_{0.5}/Mg_{2.5}(Al)O$[e]	10.3	37.1	55.3	6.14	22.2	0.25	0.90
	FCR[f]	0.43	0.71	–	–	–	0.003	0.005
	RUA[f]	1.98	8.04	–	–	–	0.149	0.605

[a] Steaming was carried out at 900 °C for 10 h in a mixed gas flow of $H_2/H_2O/N_2$ (20/100/25 $ml\ min^{-1}$). The catalysts were used as the powders of 0.075–0.180 mmΦ.

[b] Steam reforming of methane was carried out between 500–600 °C in a mixed gas flow of $CH_4/H_2O/N_2$ (88.8/177.6/44.4 $ml\ min^{-1}$) at the GHSV of 1.6×10^6 $ml\ g_{cat}^{-1}\ h^{-1}$ e or 3.6×10^5 $ml\ g_{cat}^{-1}\ h^{-1}$ f after prereduction at 900 °C for 0.5 h.

[c] TOF value was calculated based on surface Ni amount.

[d] TOF value was calculated based on total Ni amount.

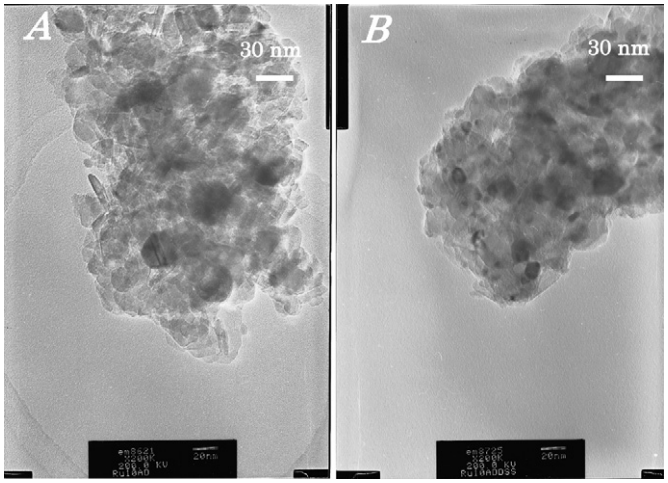

Fig. 8. TEM images of the 0.10 wt% Ru–$Ni_{0.5}/Mg_{2.5}$(Al)O catalyst after the steaming at 900 °C (A) and after the steaming at 900 °C, followed by the SRM DSS at 700 °C.

lines of Ni metal together with the lines of both Mg(Ni,Al)O periclase and Mg(Ni)Al_2O_4 spinel were strengthened on both catalysts after steaming (Figs. 7b and 7e). The particle sizes of the Ni metal were calculated based on both XRD and H_2 uptake measurements (Table 1), clearly showing heavy sintering of the Ni metal particles after steaming. Moreover, a TEM image of the 0.10 wt% Ru–$Ni_{0.5}/Mg_{2.5}$(Al)O catalyst showed ca. 36 nm of the Ni metal particles at the maximum (Fig. 8A), also clearly demonstrating heavy sintering after steaming.

XRD patterns of the 13.5 wt% Ni/γ-Al_2O_3, FCR, and RUA catalysts before and after steaming at 900 °C are shown in Figs. 9A, 9B and 9C, respectively. The 13.5 wt% Ni/γ-Al_2O_3 catalyst showed reflection lines of both Ni metal and γ-Al_2O_3 before steaming, with the reflections of Ni metal strengthened and those of α-Al_2O_3 also appearing after steaming (Fig. 9A). This indicates that Ni metal particles were sintered (see Table 1) and part of the γ-Al_2O_3 was converted to α-Al_2O_3 during steaming at 900 °C for 10 h. For both the FCR and RUA catalysts, no significant change in the XRD patterns was observed after steaming. After the SRM DSS, both 13.5 wt% Ni/γ-Al_2O_3 and FCR showed reflection lines of NiO, indicating that Ni metal was oxidized to NiO. The RUA catalyst showed no significant change in XRD patterns, but the size of Ru metal particles increased, indicating that sintering occurred (see Table 1).

3.8. XANES and EXAFS analyses of Ru-doped Ni/Mg(Al)O catalysts

Fig. 10A shows the Ru *K*-edge XANES spectra of the 0.50 wt% Ru–$Ni_{0.5}/Mg_{2.5}$(Al)O catalyst during preparation. Ru foil as a control showed a peak at 22,123 eV, along with a preedge at 22,106 eV and a characteristic peak at the higher energy (Fig. 10A d). These values are slightly lower compared with those reported by Hosokawa et al. [34] (i.e., a preedge at 22,115 eV and a peak at 22,128 eV). After the $Mg_{2.5}$($Ni_{0.5}$,Al)O periclase powders were dipped in an aqueous solution of Ru(III) nitrate, a peak at 22,126 eV appeared along with another peak at higher energy (Fig. 10A a). An almost similar spectrum was ob-

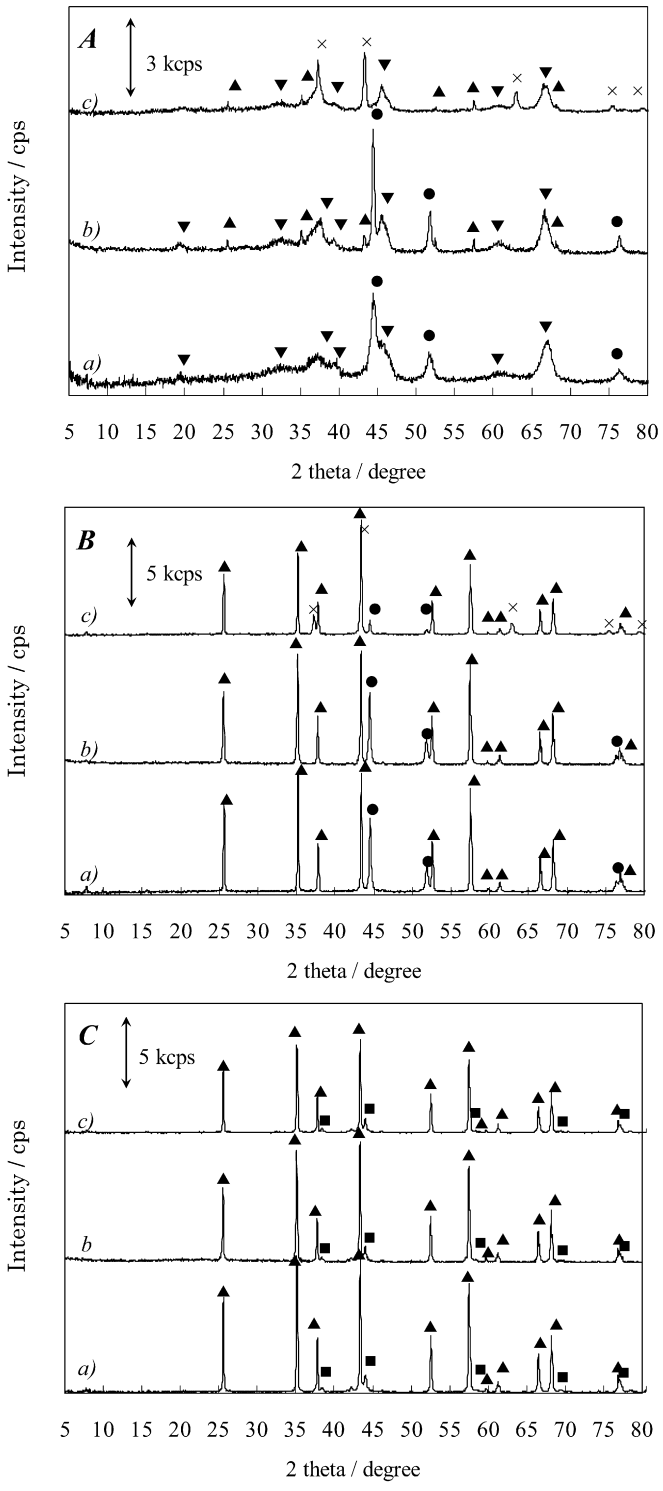

Fig. 9. XRD patterns of 13.5 wt% Ni/γ-Al_2O_3 (A), FCR (B) and RUA (C) after reduction, after steaming at 900 °C and after further followed by the steam purged SRM DSS. (a) after reduction; (b) after steaming at 900 °C; (c) after steaming at 900 °C followed by the SRM DSS. (▲) α-Al_2O_3; (▼) γ-Al_2O_3; (×) NiO; (●) Ni metal; (■) Ru metal.

tained for the sample after calcination at 900 °C (Fig. 10A b). It was reported that Ru^{4+} in strontium ruthenates showed a peak at 22,150 eV [35] and that bulk RuO_2 on Ru/CeO_2 showed a main peak between 22,130 and 22,148 eV [36]. It is likely that the Ru species was isolated on the present sample before the

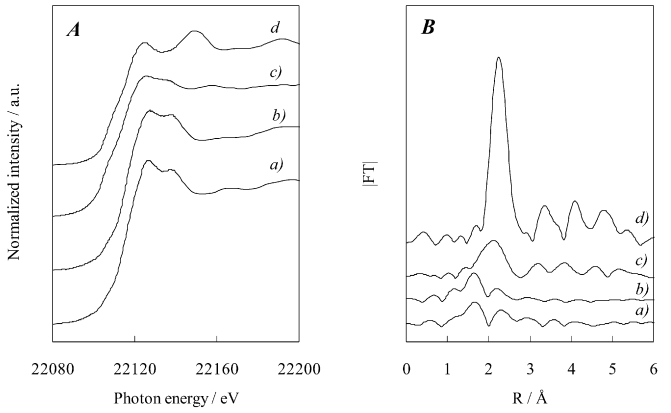

Fig. 10. Ru K-edge XANES (A) and Fourier transforms of k^3-weighted Ru K-edge EXAFS (B) spectra of 0.50 wt% Ru–$Ni_{0.5}/Mg_{2.5}$(Al)O during the preparation. (a) After dipping; (b) after calcination; (c) after reduction; (d) Ru foil.

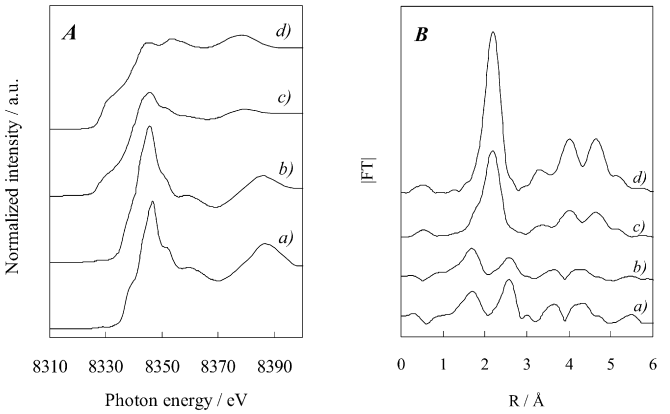

Fig. 11. Ni K-edge XANES (A) and Fourier transforms of k^3-weighted Ni K-edge EXAFS (B) spectra of 0.50 wt% Ru–$Ni_{0.5}/Mg_{2.5}$(Al)O during the preparation. (a) After dipping; (b) after calcination; (c) after reduction; (d) Ni foil.

reduction, considering their lower peak energies. After reduction, a preedge appeared at 22,106 eV, and the main peak shifted toward slightly lower energy (i.e., 22,123 eV [Fig. 10A c]), suggesting the Ru species was reduced to metallic state and still isolated, because the peak energy was lower than that of Ru foil.

Fig. 10B shows the Fourier transforms of k^3-weighted Ru K-edge EXAFS spectra of the 0.50 wt% Ru–$Ni_{0.5}/Mg_{2.5}$(Al)O catalyst during preparation along with that of Ru foil as a control. The Ru foil showed a peak at 2.26 Å (non-phase shift corrected), corresponding to the Ru–Ru bond in metallic Ru (Fig. 10B d) [34]. After $Mg_{2.5}(Ni_{0.5},Al)O$ periclase powders were dipped in aqueous solution of Ru(III) nitrate, a peak at 1.62 Å (non-phase shift corrected) appeared and remained after calcination at 900 °C (Fig. 10B a and b). A weak peak observed at around 400 °C in the TPR of the 0.50 wt% Ru–$Ni_{0.5}/Mg_{2.5}$(Al)O catalyst [24] can be ascribed to the reduction of RuO_2 to Ru metal, because no other stable ruthenium oxides are known to exist in the solid state [37,38]. This indicates that part of the Ru was separated as RuO_2 from the Ru–Ni binary system. Hosokawa et al. [36] observed a peak at 3.0 Å (non-phase shift corrected) for bulk RuO_2 supported on CeO_2 and ascribed it to Ru–Ru bonding in the bulk RuO_2. In the present work, we observed no such peak (Fig. 10B a and b), suggesting that RuO_2 was dispersed and isolated on the present catalyst. After reduction, a new peak appeared at 2.08 Å (non-phase shift corrected) (Fig. 10B c) that was smaller than the distance of the Ru–Ru bonding, suggesting that the Ru atom bonded mainly to the Ni atom.

In the Ni K-edge XANES spectra of the 0.50 wt% Ru–$Ni_{0.5}/Mg_{2.5}$(Al)O catalyst, a preedge at 8338 eV and a peak at 8347 eV, along with three peaks at higher energy, were observed after both dipping and calcination (Figs. 11A a and 11 b). The peak shape closely resembled that of the mixture of NiO and $NiAl_2O_4$ between 8335 and 8345 eV reported by Hungría et al. [39]. To the best of our knowledge, no previous studies have reported on the XANES of Ni in Mg(Ni,Al)O periclase. Because Ni^{2+} has octahedral coordination in both NiO and Mg(Ni,Al)O periclase, a similar peak can be observed for both samples. Moreover, a certain amount of $NiAl_2O_4$ must be produced during calcination at 900 °C, as was detected by XRD (Fig. 7). In the Fourier transforms of k^3-weighted Ni K-edge EXAFS spectra, two peaks were observed at 1.66 and 2.56 Å (both non-phase shift corrected) for both samples after dipping and after calcination (Fig. 11B a and b). Hungría et al. [39] reported that two peaks were observed at 1.65 and 2.56 Å (both non-phase shift corrected) for the FT EXAFS of NiO. The peak intensity ratio of the latter to the former was 0.57 in the calcined sample (Fig. 11B b) and was calculated as 4.03 for NiO based on the results on Hungría et al. [39]. The former and latter peaks can be assigned to Ni–O and Ni–Ni bonding, respectively, because the population of Ni–Ni bonding must be smaller for $Mg_{2.5}(Ni_{0.5},Al)O$ periclase than for NiO. After the reduction, both peaks at 1.66 and 2.56 Å disappeared and a new peak appeared at 2.13 Å (non-phase shift corrected) (Fig. 11B c), coinciding with that observed for Ni foil as a control (Fig. 11B d). This bond distance coincided with the value for Ni metal reported by Juan-Juan et al. [40] and clearly showed that Ni^{2+} in $Mg_{2.5}(Ni_{0.5},Al)O$ periclase was reduced to Ni metal. Ru apparently showed no effect on the spectra of Ni, because the molar amount was too small (i.e., 1/55) compared with Ni in the 0.5 wt% Ru–$Ni_{0.5}/Mg_{2.5}$(Al)O catalyst.

4. Discussion

4.1. Surface structure of Ru-doped Ni/Mg(Al)O catalysts

The curve-fitting results of the Ni K-edge and Ru K-edge EXAFS are summarized in Tables 3 and 4, respectively. In the results of the Ni K-edge EXAFS (Table 3), total coordination number for the Ni–O shell must be 6 before the reduction, whereas that for Ni–Ni shell must be 12 if Ni exists as bulk Ni metal after reduction. The incipient wetness preparation method did have as much of an affect on the coordination atmosphere around Ni^{2+} in the 0.50 wt% Ru–$Ni_{0.5}/Mg_{2.5}$(Al)O catalyst; almost the same coordination number was observed for the catalyst prepared with 5 ml of Ru(III) nitrate aque-

Table 3
Curve fitting results of Ni K-edge EXAFS after calcination and reduction[a]

Sample	Shells	C.N.	R (Å)	σ (Å)	ΔE_0 (eV)	R_f (%)
0.50 wt% Ru–$Ni_{0.5}/Mg_{2.5}$(Al)O[b]	Ni–Ni	7.2 ± 0.3	2.49 ± 0.002	0.064 ± 0.003	-1.6 ± 0.6	3.5
	Ni–O	1.5 ± 0.5	2.02 ± 0.020	0.069 ± 0.027	-1.4 ± 5.6	
0.50 wt% Ru–$Ni_{0.5}/Mg_{2.5}$(Al)O[c]	Ni–O	5.7 ± 0.4	2.08 ± 0.006	0.078 ± 0.007	-5.7 ± 1.2	5.4
0.50 wt% Ru–$Ni_{0.5}/Mg_{2.5}$(Al)O[c,d]	Ni–O	5.8 ± 0.3	2.09 ± 0.005	0.073 ± 0.007	-6.8 ± 1.1	7.1
NiO[e]	Ni–O	6	2.02	–	–	–
Ni foil[e]	Ni–Ni	12	2.49	–	–	–

[a] C.N., coordination number; R, bond length (Å); ΔE_0, difference in the origin of photoelectron energy between the reference and the sample; σ, Debye–Waller factor (Å); R_f, residual factor.
[b] After reduction.
[c] After calcination.
[d] Prepared by iw method using 0.4 ml of Ru nitrate aqueous solution.
[e] Data from X-ray crystallography.

Table 4
Curve fitting results of Ru K-edge EXAFS after calcination and reduction[a]

Sample	Shells	C.N.	R (Å)	σ (Å)	ΔE_0 (eV)	R_f (%)
0.50 wt% Ru–$Ni_{0.5}/Mg_{2.5}$(Al)O[b]	Ru–Ni	3.5 ± 0.8	2.46 ± 0.018	0.098 ± 0.022	-9.1 ± 3.3	2.3
	Ru–Ru	1.6 ± 0.9	2.67 ± 0.025	0.084 ± 0.033	-5.4 ± 5.7	
0.50 wt% Ru–$Ni_{0.5}/Mg_{2.5}$(Al)O[c]	Ru–O	2.8 ± 0.3	2.04 ± 0.006	0.021 ± 0.018	0.1 ± 1.7	5.0
0.50 wt% Ru–$Ni_{0.5}/Mg_{2.5}$(Al)O[c,d]	Ru–O	4.4 ± 0.5	2.08 ± 0.011	0.087 ± 0.015	6.4 ± 2.1	4.3
RuO_2	Ru–O	6	–	–	–	–
Ru foil	Ru–Ru	12	2.66	–	–	–

[a] C.N., coordination number; R, bond length (Å); ΔE_0, difference in the origin of photoelectron energy between the reference and the sample; σ, Debye–Waller factor (Å); R_f, residual factor.
[b] After reduction.
[c] After calcination.
[d] Prepared by iw method using 0.4 ml of Ru nitrate aqueous solution.

ous solution. Before the reduction, Ni^{2+} in both catalysts was almost fully coordinated with oxygen atoms. After the reduction, Ni^{2+} was substantially reduced to Ni metal, but the Ni–O shell was still observed, because the reduction was not completed in $Mg_{2.5}(Ni_{0.5},Al)O$ periclase due to its reduction of ca. 80% [15,31]. In the curve-fitting results of the Ru K-edge EXAFS (Table 4), the total coordination number for the Ru–O shell was 6 if the Ru existed as bulk RuO_2 before the reduction, whereas that for the Ru–Ru shell was 12 if the Ru existed as bulk Ru metal after the reduction. The incipient wetness preparation technique afforded higher coordination numbers than the preparation with 5 ml of Ru(III) nitrate aqueous solution, indicating that RuO_2 existed as larger particles in the former method compared with the latter method. Compared with the values obtained for Ni (Table 3), the coordination numbers were much smaller for Ru. Especially after reduction, the total coordination number decreased; moreover, the Ru–Ni bonding was more abundant as a main shell compared with that of Ru–Ru bonding, judging from the spectrum in Fig. 10B c. This strongly indicates that the Ru was located in the surface layer of finely dispersed Ni metal particles after reduction.

After steaming, curve fitting was successfully carried out for the Ni K-edge EXAFS but was difficult to accomplish for the Ru K-edge EXAFS. This is probably due to the fact that phase separation between Ru and Ni metal occurred, as was later demonstrated in the TPR results (vide infra).

4.2. Active sites on Ru-doped Ni/Mg(Al)O catalysts

Previously [24], we suggested that RuNi alloy was formed and the size of Ni metal particles was decreased by Ru doping on the $Ni_{0.5}/Mg_{2.5}$(Al)O catalysts. H_2 uptake was dramatically increased by Ru doping on the $Ni_{0.5}/Mg_{2.5}$(Al)O catalyst; increased Ru doping led to a significant increase in H_2 uptake but a decrease in metallic Ni particle size. The contribution of Ru itself to the H_2 uptake on the Ru–$Ni_{0.5}/Mg_{2.5}$(Al)O catalysts must have been slight, because the H_2 uptake was very low on the 0.10 wt% Ru/Mg_3(Al)O catalyst [24] and the molar ratio of Ru/Ni was as low as 1/275 for the 0.1 wt% Ru–$Ni_{0.5}/Mg_{2.5}$(Al)O catalyst.

Basile et al. [41] reported that Rh was completely soluble but Ru was not soluble in a Mg(Al)O periclase phase with a high Mg/Al ratio. It is likely that Ru^{3+} remained as a separate phase from the Mg(Ni)–Al HT structure reconstituted from Mg(Ni,Al)O periclase during preparation. The EXAFS data suggested that Ru was located in the surface layer of Ni metal particles, apparently reflecting the inability of Ru^{3+} to enter into the Mg(Ni)–Al HT structure [41]. Ru^{3+} ions were separated from Mg(Ni,Al)O periclase; thus, Ru^{3+} and Ni^{2+} were reduced separately at the first step. However, as previously reported in the TPR results of Ru-doped Ni/Mg(Al)O catalysts [15,25], Ru actually assists in the reduction of oxidized Ni, pulling it out of the mixed oxide [i.e., Mg(Al,Ni)O periclase] through some sort of hydrogen-spillover mechanism. Simulta-

neously with the Ni reduction, surface RuNi alloy formation can occur on the fine Ni metal particles. We can conclude that the active sites on the catalyst are the RuNi alloys on fine Ni metal particles.

4.3. Sustainability of Ru-doped Ni/Mg(Al)O catalyst

Our results clearly demonstrate that the passivated 0.10 wt% Ru–$Ni_{0.5}/Mg_{2.5}$(Al)O catalyst by steaming was not deactivated in both the stationary and DSS operations of SRM, although the other catalysts were certainly deactivated in either the stationary or the DSS operation (Figs. 3 and 5). After SRM DSS of the passivated Ni catalysts, the Ni metal particle size decreased in both the $Ni_{0.5}/Mg_{2.5}$(Al)O and 0.10 wt% Ru–$Ni_{0.5}/Mg_{2.5}$(Al)O catalysts (Table 1). Comparing the XRD patterns of the passivated 0.10 wt% Ru–$Ni_{0.5}/Mg_{2.5}$(Al)O catalyst before and after SRM DSS (Figs. 7e and 7f) with those of the passivated $Ni_{0.5}/Mg_{2.5}$(Al)O catalyst before and after SRM DSS (Figs. 7b and 7c) shows that in both catalysts, the reflection lines of Ni metal were significantly weakened after the SRM DSS. This suggests that part of the Ni metal was oxidized to Ni^{2+} and incorporated into the Mg(Ni,Al)O periclase, because no reflection of NiO was observed in either pattern. In contrast, after SRM DSS, the Ni metal particle size increased for the FCR catalyst (Table 1). Both passivated 13.5 wt% Ni/γ-Al_2O_3 and FCR catalysts clearly showed NiO reflections after SRM DSS (Figs. 9A and 9B). The reflection lines of Ni metal remained on the passivated FCR catalyst, whereas no such line could be seen on the passivated 13.5 wt% Ni/γ-Al_2O_3 catalyst. This suggests that only the surface layer of Ni metal particles was oxidized on the passivated FCR catalyst, whereas Ni metal particles were totally oxidized on the passivated 13.5 wt% Ni/γ-Al_2O_3 catalyst. In fact, all of the passivated $Ni_{0.5}/Mg_{2.5}$(Al)O, 13.5 wt% Ni/γ-Al_2O_3 and FCR catalysts were totally deactivated after the first steam purging in SRM DSS due to the oxidation of either surface Ni metal or total Ni metal on the catalysts.

Although the RUA catalyst showed no distinct change in XRD pattern during SRM DSS (Fig. 9C), the Ru metal particle size increased after SRM DSS, suggesting a weakness of Ru catalysts against steam purging. Note that the 0.10 wt% Ru–$Ni_{0.5}/Mg_{2.5}$(Al)O catalyst alone showed outstanding behavior, and, interestingly, the particle size of Ni metal decreased close to the original value and simultaneously the activity was sustained during SRM DSS. Such a size decrease (i.e., redispersion of the sintered Ni metal particles) could be clearly seen in both the XRD patterns (Fig. 7f) and the TEM images of the 0.10 wt% Ru–$Ni_{0.5}/Mg_{2.5}$(Al)O catalyst passivated by steaming followed by SRM DSS (Fig. 8B); the maximum size of the Ni metal particles was ca. 15 nm, far smaller than that before SRM DSS (ca. 36 nm) (Fig. 8A).

4.4. Regenerative activity of Ru-doped Ni/Mg(Al)O catalysts

TPR measurements were carried out for the passivated 0.10 wt% Ru–$Ni_{0.5}/Mg_{2.5}$(Al)O and passivated $Ni_{0.5}/Mg_{2.5}$(Al)O catalysts before and after SRM DSS. TPR curves of both fresh 0.10 wt% Ru–$Ni_{0.5}/Mg_{2.5}$(Al)O and $Ni_{0.5}/Mg_{2.5}$(Al)O catalysts after calcination at 850 °C are shown in Figs. 12d and 12a. A single peak of the $Ni^{2+} \rightarrow Ni^0$ reduction was observed at 887 and 849 °C as reported previously, indicating that Ru assisted in the reduction of Ni^{2+} in $Mg_{2.5}(Ni_{0.5},Al)O$ periclase [15,25]. After steaming at 900 °C, the reduction peak was separated into two main temperature areas, one at the higher temperature (A) and another at the far lower temperature (B). It seems that Mg(Ni,Al)O periclase was reductively decomposed to large-sized Ni metal particles and the periclase of lower Ni content after steaming of the $Ni_{0.5}/Mg_{2.5}$(Al)O catalyst (Fig. 12b). Part of the Ni^{2+} in the $Mg_{2.5}(Ni_{0.5},Al)O$ periclase was first reduced to Ni metal particles; this was then further exposed to the steaming atmosphere, after which it grew to the isolated large-sized Ni metal particles. Simultaneously the Mg(Ni,Al)O periclase lost a part of the Ni species and was exposed to the steaming atmosphere to form the sintered structure having hardly reducible Ni species. The peaks B at 290 and 328 °C can be assigned to the isolated Ni metal particles, whereas the peak A at 941 °C can be assigned to the hardly reducible Ni species in the sintered periclase (Fig. 12b). A similar phase separation occurred in the presence of Ru; peak B appeared at an even lower temperature and was subdivided into three peaks at 147, 199, and 254 °C, whereas peak A shifted to 888 °C (Fig. 12e). This likely indicates that phase separation of NiRu alloy occurred, because it was reported that Ru exhibited reduction peaks at 140–200 °C, whereas Ni reduction appeared at 230–300 °C in the TPR of supported metal catalysts [42,43]. When the passivated $Ni_{0.5}/Mg_{2.5}$(Al)O catalyst was exposed to SRM DSS, the peak B disappeared, whereas the peak A again shifted toward lower temperature (839 °C) but with the shoulder remaining at 941 °C (Fig. 12c). On the other hand, after SRM DSS of the passivated 0.10 wt% Ru–$Ni_{0.5}/Mg_{2.5}$(Al)O catalyst, peak B shifted toward higher temperatures of 279 °C and 326 °C, whereas peak A completely shifted toward a lower tem-

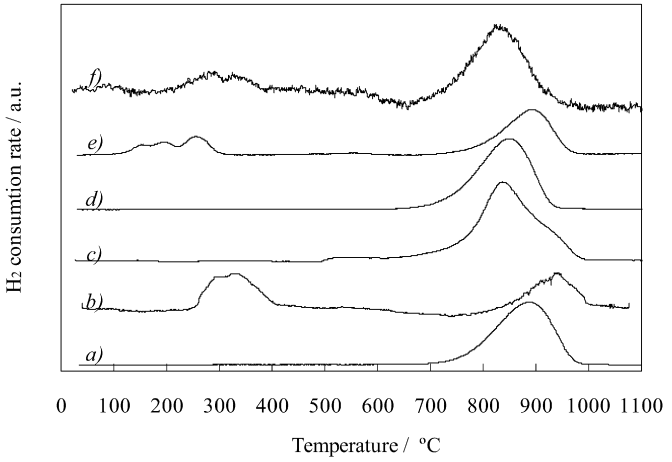

Fig. 12. TPR profiles of $Ni_{0.5}/Mg_3$(Al)O and 0.10 wt% Ru–$Ni_{0.5}/Mg_{2.5}$(Al)O catalysts after the reduction, after the steaming at 900 °C and after followed by the steam purged SRM DSS at 700 °C. (a) $Ni_{0.5}/Mg_{2.5}$(Al)O after the reduction; (b) $Ni_{0.5}/Mg_{2.5}$(Al)O after the steaming at 900 °C; (c) $Ni_{0.5}/Mg_{2.5}$(Al)O after the SRM DSS at 700 °C; (d) 0.10 wt% Ru–$Ni_{0.5}/Mg_{2.5}$(Al)O after the reduction; (e) 0.10 wt% Ru–$Ni_{0.5}/Mg_{2.5}$(Al)O after the steaming at 900 °C; (f) 0.10 wt% Ru–$Ni_{0.5}/Mg_{2.5}$(Al)O after the SRM DSS at 700 °C.

perature of 826 °C (Fig. 12f). These findings suggest that the separated species were again combined and reconstituted to the original phase on the 0.10 wt% Ru–$Ni_{0.5}/Mg_{2.5}$(Al)O catalyst.

The TPR results given above, along with the XRD (Fig. 7f) and TEM (Fig. 8B) observations of the 0.10 wt% Ru–$Ni_{0.5}/Mg_{2.5}$(Al)O catalyst passivated by steaming followed by SRM DSS, seem to be important for understanding the catalytic mechanism. Even after severe passivation by steaming at 900 °C, the sintered Ni metal particles were redispersed, and the original active sites were regenerated during SRM DSS in the presence of Ru. The sintered Ni metal particles must be oxidized to Ni^{2+} by steam and possibly incorporated into Mg(Ni,Al)O periclase. In turn, Ni^{2+} in Mg(Ni,Al)O periclase can be quickly reduced, assisted by hydrogen spillover on Ru metal or Ru–Ni alloy. Such reduction–oxidation between Ni^0 and Ni^{2+} on/in Mg(Ni,Al)O periclase aided by hydrogen spillover on Ru metal or RuNi alloy effectively contributed to the regeneration of activity on the Ru-doped Ni/Mg(Al)O catalysts during the SRM DSS operation.

It seems that Mg(Al)O periclase plays an important role in the self-regenerative activity of Ru-doped Ni/Mg(Al)O catalyst. First, Ni^{2+} in Mg(Al,Ni)O periclase is reduced by hydrogen spillover from Ru metal to form Ru–Ni alloy on the surface of metallic Ni particles. When surface oxidation occurs on metallic Ni particles during SRM DSS, it probably starts at the periphery between metallic Ni particles and Mg(Al)O periclase as the support and gradually proceeds to the bulk of the particles. At the same time, Ni^{2+} thus formed must be reincorporated into the lattice of Mg(Al,Ni)O periclase (Scheme 1). No NiO formation was observed on the Ru-doped Ni/Mg(Al)O catalyst during this procedure. The $Ni_{0.5}/Mg_{2.5}$(Al)O catalyst showed no NiO formation and also demonstrated no self-regenerative activity, due to inability to reduce Ni^{2+}. In contrast, both FCR and 13.5 wt% Ni/γ-Al_2O_3 produced NiO. In all likelihood, NiO cannot be reductively redispersed to fine metallic Ni particles even in the presence of Ru, although this hypothesis must be verified concretely by experiments. It is most likely that the crystal structure of Mg(Al,Ni)O periclase plays an important role in the self-regenerative activity assisted by Ru on the Ru-doped Ni/Mg(Al)O catalyst.

5. Conclusion

Ni/Mg(Al)O catalyst was doped with trace Ru and tested in the steam-purged DSS operation of SRM at 200–700 °C. Highly dispersed Ru/Ni bimetal supported catalysts were obtained, and Ru–Ni alloy was formed on the surface of fine Ni metal particles on the catalysts. The Ru–Ni/Mg(Al)O catalysts exhibited self-regenerative activity aided by both trace Ru and Mg(Ni,Al)O periclase structure during the DSS operation; trace Ru or Ru–Ni alloy aided the regeneration of Ni metal from the Ni^{2+} in the periclase by hydrogen spillover. Even sintered Ni metal particles on the Ni/Mg(Al)O catalyst by steaming at 900 °C for 10 h were redispersed, resulting in high and stable activity in the presence of trace Ru. Such prominent catalytic performance of the Ru–Ni/Mg(Al)O system is likely to be achieved by the continuous self-regeneration of active Ni metal species assisted cooperatively by both hydrogen spillover via trace Ru metal or Ru–Ni alloy and reversible reduction–oxidation between $Ni^0 \leftrightarrow Ni^{2+}$ in the Mg(Ni,Al)O periclase.

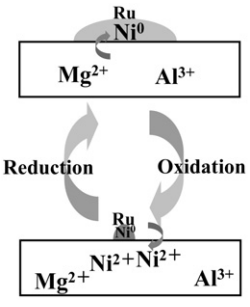

Scheme 1. Self-regenerative activity of Ru-doped Ni/Mg(Al)O catalyst.

References

[1] J.R. Rostrup-Nielsen, Catal. Today 71 (2002) 243.
[2] T. Shishido, M. Sukenobu, H. Morioka, R. Furukawa, H. Shirahase, K. Takehira, Catal. Lett. 73 (2001) 21.
[3] T. Shishido, M. Sukenobu, H. Morioka, M. Kondo, Y. Wang, K. Takaki, K. Takehira, Appl. Catal. A 223 (2002) 35.
[4] K. Takehira, T. Shishido, P. Wang, T. Kosaka, K. Takaki, Phys. Chem. Chem. Phys. 5 (2003) 3801.
[5] K. Takehira, T. Shishido, P. Wang, T. Kosaka, K. Takaki, J. Catal. 221 (2004) 43.
[6] K. Takehira, T. Shishido, D. Shouro, K. Murakami, M. Honda, T. Kawabata, K. Takaki, Appl. Catal. A 279 (2005) 41.
[7] A.I. Tsyganok, M. Inaba, T. Tsunoda, K. Uchida, K. Suzuki, K. Takehira, T. Hayakawa, Appl. Catal. A 292 (2005) 328.
[8] K. Takehira, T. Kawabata, T. Shishido, K. Murakami, T. Ohi, D. Shoro, M. Honda, K. Takaki, J. Catal. 231 (2005) 92.
[9] S. Wang, H.Y. Zhu, G.Q. Lu, J. Colloid Interface Sci. 204 (1998) 128.
[10] V.A. Tsipouriari, Z. Zhang, X.E. Verykios, J. Catal. 179 (1998) 283.
[11] H.S. Bengaard, J.K. Nørskov, J. Sehested, B.S. Clausen, L.P. Nielsen, A.M. Molenbroek, J.R. Rostrup-Nielsen, J. Catal. 209 (2002) 365.
[12] S. Natesakhawat, R.B. Watson, X. Wang, U.S. Ozkan, J. Catal. 234 (2005) 496.
[13] T. Ohi, T. Miyata, D. Li, T. Shishido, T. Kawabata, T. Sano, K. Takehira, Appl. Catal. A 308 (2006) 194.
[14] T. Miyata, D. Li, M. Shiraga, T. Shishido, Y. Oumi, T. Sano, K. Takehira, Appl. Catal. A 310 (2006) 97.
[15] T. Miyata, M. Shiraga, D. Li, I. Atake, T. Shishido, Y. Oumi, T. Sano, K. Takehira, Catal. Commun. 8 (2007) 447.
[16] F. Basile, G. Fornasari, F. Trifirò, A. Vaccari, Catal. Today 77 (2002) 215.
[17] K. Nagaoka, A. Jentys, J.A. Lercher, J. Catal. 229 (2005) 185.
[18] M. Nurunnabi, B. Li, K. Kunimori, K. Suzuki, K. Fujimoto, K. Tomishige, Appl. Catal. A 292 (2005) 272.
[19] M. Nurunnabi, K. Fujimoto, K. Suzuki, B. Li, S. Kado, K. Kunimori, K. Tomishige, Catal. Commun. 7 (2006) 73.
[20] M. Nurunnabi, Y. Mukainakano, S. Kado, B. Li, K. Kunimori, K. Suzuki, K. Fujimoto, K. Tomishige, Appl. Catal. A 299 (2006) 145.
[21] J.A.C. Dias, J.M. Assaf, J. Power Sources 130 (2004) 106.
[22] J.A.C. Dias, J.M. Assaf, J. Power Sources 139 (2005) 176.
[23] J.H. Jeong, J.W. Lee, D.J. Seo, Y. Seo, W.L. Yoon, D.K. Lee, D.H. Kim, Appl. Catal. A 302 (2006) 151.
[24] M. Shiraga, D. Li, I. Atake, T. Shishido, Y. Oumi, T. Sano, K. Takehira, Appl. Catal. A 318 (2007) 143.
[25] D. Li, M. Shiraga, I. Atake, T. Shishido, Y. Oumi, T. Sano, K. Takehira, Appl. Catal. A 321 (2007) 155.
[26] J.W. Cook, D.E. Sayers, J. Appl. Phys. 52 (1981) 5024.
[27] A.L. Ankudinov, B. Ravel, J.J. Rehr, S.D. Conradson, Phys. Rev. B 58 (1998) 7565.
[28] C.H. Bartholomew, R.B. Pannell, J.L. Butler, J. Catal. 65 (1980) 335.

[29] N. Sahli, C. Petit, A.C. Roger, A. Kiennemann, S. Libs, M.M. Bettahar, Catal. Today 113 (2006) 187.

[30] J. Okal, M. Zawadzki, L. Kępiński, L. Krajczyk, W. Tylus, Appl. Catal. A 319 (2007) 202.

[31] A. Olafsen, Å. Slagtern, I.M. Dahl, U. Olsbye, Y. Schuurman, C. Mirodatos, J. Catal. 229 (2005) 163.

[32] J.H. Eun, J.H. Lee, S.G. Kim, M.Y. Um, S.Y. Park, H.J. Kim, Thin Solid Films 435 (2003) 199.

[33] M.C.J. Bradford, M.A. Vannice, Appl. Catal. A 142 (1996) 73.

[34] S. Hosokawa, S. Nogawa, M. Taniguchi, K. Utani, H. Kanai, S. Imamura, Appl. Catal. A 288 (2006) 67.

[35] M. Yoshimura, Y. Yoshida, S.I. Ikeda, N. Shirakawa, I. Nagai, S. Hara, K. Koyama, M. Nedo, Y. Uwatoko, J. Magn. Magn. Mater. 272–276 (2004) e257.

[36] S. Hosokawa, M. Taniguchi, K. Utani, H. Kanai, S. Imamura, Appl. Catal. A 289 (2005) 115.

[37] H. Madhavaram, H. Idriss, S. Wendt, Y.D. Kim, M. Knapp, H. Over, J. Aßmann, E. Löffler, M. Muhler, J. Catal. 202 (2001) 296.

[38] I. Balint, A. Miyazaki, K. Aika, J. Catal. 220 (2003) 74.

[39] A.B. Hungría, N.D. Browning, R.P. Erni, M. Fernández-García, J.C. Conesa, J.A. Pérez-Omil, A. Martínez-Arias, J. Catal. 235 (2005) 251.

[40] J. Juan-Juan, M.C. Román-Martínez, M.J. Illán-Gómez, Appl. Catal. A 301 (2006) 9.

[41] F. Basile, G. Fornasari, V. Rosetti, F. Trifirò, A. Vaccari, Catal. Today 91–91 (2004) 293.

[42] M.B.I. Choudhury, S. Ahmed, M.A. Shalabi, T. Inui, Appl. Catal. A 314 (2006) 47.

[43] C. Crisafulli, S. Sciré, S. Minicò, L. Solarino, Appl. Catal. A 225 (2002) 1.